Available online at www.sciencedirect.com
ScienceDirect
Inorganica Chimica Acta 360 (2007) 2245–2254
Inorganica Chimica Acta
www.elsevier.com/locate/ica

# A nickel(II) di-$\mu_2$-phenolato bridged dinuclear complex: Weak antiferromagnetic interactions in nickel(II) dimers

Michael J. Prushan [a,*], Diana M. Tomezsko [a,1], Sam Lofland [b], Matthias Zeller [c], Allen D. Hunter [c]

[a] Department of Chemistry and Biochemistry, La Salle University, Philadelphia, PA 19141-119, USA
[b] Department of Physics, Rowan University, Glassboro, NJ 08028, USA
[c] STaRBURSTT-Cyberdiffraction Consortium @ YSU, Department of Chemistry, Youngstown State University, Youngstown, OH 44555-3663, USA

Received 26 October 2006; accepted 5 November 2006
Available online 14 November 2006

**Abstract**

$[Ni(dpmap)(H_2O)]_2(ClO_4)_2 \cdot 3(CH_3)_2CO$, a dinuclear nickel(II) complex of 2-{[[Di(2-pyridyl)methyl](methyl)amino]methyl}phenol, ***dpmapH*** has been synthesized. X-ray diffraction analysis indicates that each nickel(II) center is coordinated by two ***dpmap***$^-$ ligands and two water molecules. The two nickel(II) centers are bridged by $\mu_2$-phenolate oxygen donors. The two nickel(II) centers each have distorted octahedral symmetry, comprised of *cis*-coordinated pyridyl nitrogen, a *tert*-amino nitrogen and a bridging phenolate oxygen. Hexacoordination is completed by an oxygen atom of a water molecule. The water molecules at each nickel center are *trans*- to each other across the $Ni_2O_2$ basal plane. The two Ni atoms are separated by 3.170 Å. Variable temperature and field magnetic measurements reveal weak antiferromagnetic coupling ($J = -0.85\ cm^{-1}$) between the nickel(II) centers. The $\chi_m T$ versus $T$ data were fit using a model, derived from Kambe's method and include zero-field splitting ($D = -1.6\ cm^{-1}$). Broken-symmetry density functional theory (BS-DFT) indicates that the weak antiferromagnetism is due to electron density delocalization onto the ligand framework and the inability of the out-of plane phenolato-bridges to mediate superexchange.


*Keywords:* Nickel; Dinuclear; Magnetic measurements; DFT; X-ray diffraction

## 1. Introduction

Dinuclear μ-*O*-nickel(II) complexes with mixed N/O donor sets have the potential to act as structural, electronic and catalytic models for urease [1–3]. The active site of urease contains two nickel(II) ions bridged by hydroxo- and carbamylated lysine carboxylate donors (Fig. 1) [4,5]. Ureases isolated from several organisms have almost identical coordination modes [4,5] and some controversy exists regarding the magnetic interactions between the nickel(II) centers. Variable-temperature magnetism on jack bean urease indicates the presence of weak antiferromagnetic coupling [6]. Other studies provide evidence to the contrary, suggesting that the nickel(II) ions are in fact uncoupled and non-interacting [7] or that the coupling is ferromagnetic *via* magnetic circular dichroism (MCD) spectroscopy [8]. When elucidating the exact nature of the interactions between the metal centers, understanding not only the role of bridging donors but of the ligand backbone is necessary. Ligands with aromatic nitrogen functionalities have the potential for delocalizing electrons and have been found to influence the magnitude and sign of the coupling between nickel(II) ions [9].

Metal complexes of phenol functionalized di-(2-pyridyl)methylamines have the potential to act as poly-nucleating ligands and also have the added feature of heterocyclic donors. This ligand system has already been used to synthesize dimeric and trimeric manganese(III)

* Corresponding author. Tel.: +1 215 951 1281; fax: +1 215 951 1772.
*E-mail address:* prushan@lasalle.edu (M.J. Prushan).
[1] Undergraduate Research Student.

0020-1693/$ - see front matter © 2006 Elsevier B.V. All rights reserved.
doi:10.1016/j.ica.2006.11.008

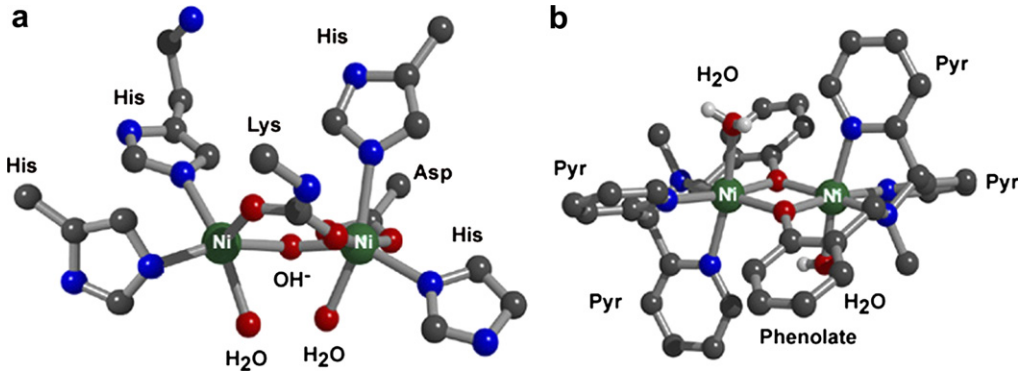


Fig. 1. (a) The urease active site, (b) the structure of $[Ni(dpmap)(H_2O)]_2^{2+}$. Coordinates for Fig. 1 derived from the crystal structure of urease from *Klebsiella aerogenes* at 2.2 Å resolution, PDB access no. 2KAU. (www.rcsb.org).

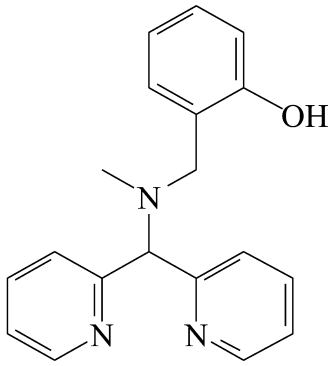


Fig. 2. Structure of 2-{[[Di(2-pyridyl)methyl](methyl)amino]methyl}phenol, ***dpmapH***.

complexes [10,11]. A manganese(II) complex of ***dpmapH*** was recently shown to be first molecular-based system which could catalytically induce movement in micro-particles [12].

Here we report the synthesis and characterization of a dinuclear nickel(II) complex with 2-{[[Di(2-pyridyl)-methyl](methyl)amino]methyl}phenol, ***dpmapH*** (Fig. 2). In the $[Ni(dpmap)(H_2O)]_2(ClO_4)_2 \cdot 3(CH_3)_2CO$ complex, the two ***dpmap***$^-$ ligands bridge two nickel(II) centers via $\mu_2$-phenolate oxygen donors. The pseudo-octahedral coordination environment is completed by water molecules bound to each nickel(II). The coordinated water molecules are *trans*- to each other across the $Ni_2O_2$ plane. Variable temperature/field magnetic measurements indicate the presence of weak antiferromagnetism between the nickel(II) centers. DFT calculations were also performed to gain insight into the nature of the coupling.

## 2. Experimental

Commercially available reagents (from Aldrich and Fisher) were used without further purification. Nickel(II) perchlorate was purchased from GFS Chemicals and used directly. 2-{[[Di(2-pyridyl)methyl](methyl)amino]methyl}-phenol, ***dpmapH*** was synthesized according to the multi-step synthesis described by La Crois [6].

### 2.1. Physical measurements

Transmissive Solid UV–Vis spectra were obtained on a Unicam UV-4 spectrophotometer of a thin coating of finely ground complex on the surface of a quartz triangle cell. Infrared spectra were collected on a Thermo Nicolet Avatar 360 FT-IR equipped also with a Nicolet Smart MIRacle ATR diamond crystal accessory. Elemental microanalysis was performed by Robertson-Microlit (Madison, NJ). FAB Mass Spectra were obtained on a VG-ZABHF high resolution double focusing instrument using 2-nitrobenzyl alcohol as the matrix at Drexel University (Philadelphia, PA).

Variable temperature/variable field magnetic measurements were obtained with a quantum design physical properties measurement system magnetometer. For variable temperature measurements (2–300 K) the applied field was 5000 Oe. Field-cooled ($H_{ac} = -0.094$ Oe) and zero-field cooled ($H_{ac} = 5000$ Oe) AC susceptibility measurements (1000 Hz oscillating frequency) were carried out between 3 and 300 K. The variable field magnetization data was measured at 3 K with an applied field between 0 and 40 000 Oe. The sample was held in a Teflon holder. Background corrections for the sample holder and diamagnetic components of the complex (Pascal's constants) were applied. Data was analyzed using Microcal Origin 6.0. Fitting iterations (200 max) utilized a combination of Levenberg-Marqardt and Simplex approaches. Molecular structures were created using PLATON 1.081 [13,14] and ARGUSLAB 4.0.1 [15] (Fig. 1).

### 2.2. Crystallographic data and refinement

The X-ray crystallographic data (Table 1) was collected of a $0.48 \times 0.43 \times 0.38$ mm piece of a large blue crystal of $[Ni(dpmap)(H_2O)]_2(ClO_4)_2 \cdot 3(CH_3)_2CO$, obtained by allowing slow evaporation of the filtrate. Diffraction data was collected with graphite-monochromatized Mo Kα X-ray radiation (fine-focus sealed tube) using a Bruker SMART CCD Diffractometer at 100(2) K. A total of 50 643 reflections were collected ($-20 \leqslant h \leqslant 20$,

Table 1
Crystallographic data

| *[Ni(dpmap)(H$_2$O)]$_2$(ClO$_4$)$_2$·3(CH$_3$)$_2$CO* | |
|---|---|
| Formula | $C_{47}H_{58}Cl_2N_6Ni_2O_{15}$ |
| Formula weight | 1135.31 |
| Crystal system | monoclinic |
| Crystal size (mm) | 0.48 × 0.43 × 0.37 |
| Space group | $P2_1/c$ |
| $a$ (Å) | 15.3547(7) |
| $b$ (Å) | 16.4544(8) |
| $c$ (Å) | 19.9011(9) |
| $\beta$ (°) | 97.6540(10) |
| $V$ (Å$^3$) | 4983.3(4) |
| $Z$ | 4 |
| $\rho_{calc}$ (g cm$^{-3}$) | 1.513 |
| $F$(000) | 2368 |
| $\mu$ (mm$^{-1}$) | 0.937 |
| $\lambda$(Mo Kα) (Å) | 0.71073 |
| $T$ (K) | 100(2) |
| $R^a$, $R_w{}^b$ | 0.0428, 0.0952 |

[a] $R = \sum\|F_o| - |F_c\|/\sum|F_o|$.
[b] $R_w = [\sum w(|F_o| - |F_c|)^2/\sum w(F_o)^2]^{1/2}$.

$-21 \leqslant k \leqslant 21$, $-26 \leqslant l \leqslant 26$) in the range of 1.34–28.28°, with 12 731 unique reflections ($R_{int} = 2.38\%$). Data was collected using the SMART (Bruker, 1997) software package; subsequent cell refinement and data reduction were accomplished with the SAINT (Bruker, 1997) software package [16]. The structure was solved and refined with using SHELXS97 (Sheldrick, 1997) and SHELXTL [17]. Water hydrogen atoms were located in the density Fourier map. Their O–H distances have been restrained to 0.84 Å within a standard deviation of 0.02, and the H···H distances have been restrained to be equal within a standard deviation of 0.02. All other hydrogen atoms were placed in calculated positions, and all hydrogen atoms were refined with an isotropic displacement parameter 1.5 (methyl, water) or 1.2 times (all others) that of the adjacent carbon or oxygen atom. Thermal ellipsoids are displayed at the 30% probability level for clarity, and hydrogen atoms are shown as spheres of arbitrary size.

### 2.3. Computational methodology

Density functional theory calculations were performed using the ORCA program developed by Nesse [18] on a 2.6 GHz Pentium 4 PC running Windows *XP*. The spin-unrestricted, Broken-Symmetry calculations were performed on a model $[Ni(dpmap)(H_2O)]_2^{2+}$ dication constructed from the X-ray crystallographic coordinates (*vide supra*). The single-point calculations were performed using the *BP86* exchange and correlation functional method, for the local density approximation (LDA) portion of the gradient-corrected (GCA) functionals, PW91 [19] was utilized. The triple-ζ Slater-type (TZV(P)) orbital basis set [20,21] was used for all atoms and the TZV/$J$[2] [22,23] auxiliary basis set was applied to the resolution of identity approximation (RI-approximation) [24–26]. The broken symmetry (BS) magnetic coupling constant was obtained using the Yamaguchi formalism [27], $J = -\frac{(E_{HS}-E_{BS})}{\langle S^2\rangle_{HS}-\langle S^2\rangle_{BS}}$, using a Spin-Hamiltonian analysis based on $\mathscr{H} = -2J\widehat{S}_1\cdot\widehat{S}_2$. Orbitals were plotted using Molkel [28,29] using an isodensity value of 0.04 au. Convergence in the self-consistent field (scf) calculations was signaled by an energy change of $10^{-6}$ Hartree, a change in the density elements matrix of $10^{-5}$ and a value of $10^{-6}$ Hartree for the maximum element of the direct inversion of iterative subspace error (DIIS).

[2] The Ahlrichs auxiliary basis sets were obtained from the TurboMole basis set library under ftp. chemie.uni-karlsruhe.de/pub/jbasen.

### 2.4. Synthesis

*[Ni(dpmap)(H$_2$O)]$_2$(ClO$_4$)$_2$·3(CH$_3$)$_2$CO.* Excess triethylamine (67 μL) was added to a lilac solution, prepared by the addition of Ni(ClO$_4$)$_2$·6H$_2$O (1 mmol, 0.362 g) to a stirring solution of 2-{[[Di(2-pyridyl)methyl](methyl)-amino]methyl}phenol, ***dpmapH*** (1 mmol, 0.101 g) in acetone (5.0 mL). The resulting turbid blue-green solution afforded a pale blue-green precipitate upon gentle heating (5 min, maintaining the liquid level by addition of more acetone). The solution was allowed to cool to room temperature and the precipitate was collected *via* vacuum filtration. Recrystallization from hot acetone afforded 1.64 g, (73%) of a pale blue crystalline solid. *Anal.* Calc. for $C_{47}H_{58}Cl_2N_6Ni_2O_{15}$: C, 49.72; H, 5.15; N, 7.40. Found: C, 49.43; H, 5.01; N, 7.43%. FAB-MS: $(M-ClO_4)^+$: 824.6 (see Fig. 3 for complete spectrum).

*Caution:* Although the complexes reported do not appear to be mechanically sensitive, perchlorate complexes should be treated with due caution.

## 3. Results and discussion

### 3.1. Description of the structure

The molecular structure of [Ni(dpmap)(H$_2$O)]$_2$(ClO$_4$)$_2$·3(CH$_3$)$_2$CO is shown in Fig. 4 (only cation shown). Selected bond lengths and angles are summarized in Table 2. The structure of the dimeric complex cation is formed by two Ni(II) ions (Ni1 and Ni2), two ***dpmap***$^-$ ligands and two water molecules. The two nickel(II) centers are bridged by μ$_2$-phenolate oxygen donors (O11 and O12). The two nickel(II) centers each have distorted octahedral symmetry, comprised of *cis*-coordinated pyridyl nitrogen (N5, N3 and N6, N4), a *tert*-amino nitrogen (N2, N1) and a bridging phenolate oxygen (O11, O12). Hexacoordination is completed by an oxygen atom of a water molecule (O9, O10). The water molecules at each nickel center are *trans*-to each other across the Ni$_2$O$_2$ basal plane. The two Ni atoms are separated by 3.170 Å with bridge angles ($\theta$) of 101.32° (Ni1–O11–Ni2) and 102.07° (Ni1–O12–Ni2), whereas the apical bond angles are 169.42° (N3–Ni1–O9) and 168.52° (N4–Ni2–O10). The phenolato-rings are above (O12–C1) and below (O–C21) the Ni$_2$O$_2$ basal plane, where the dihedral angles ($\phi$) are 15.35° and −14.17°, respectively (Fig. 5).

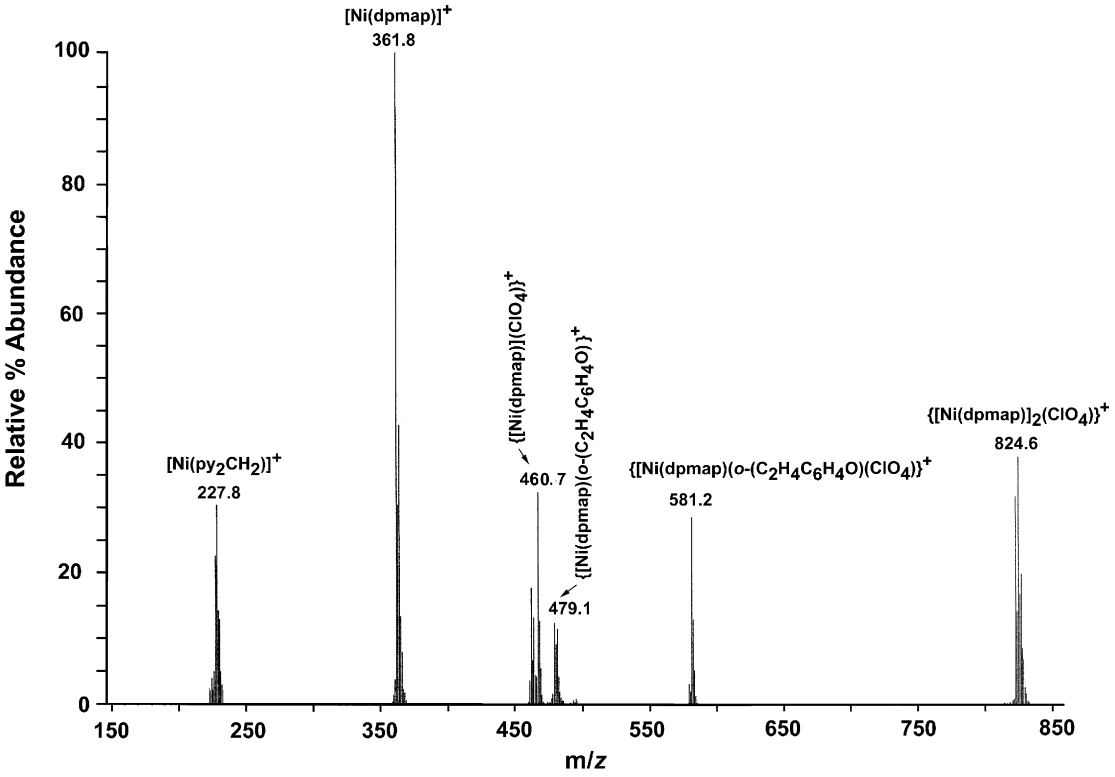


Fig. 3. FAB-MS of $[Ni(dpmap)(H_2O)]_2(ClO_4)_2 \cdot 3(CH_3)_2CO$.

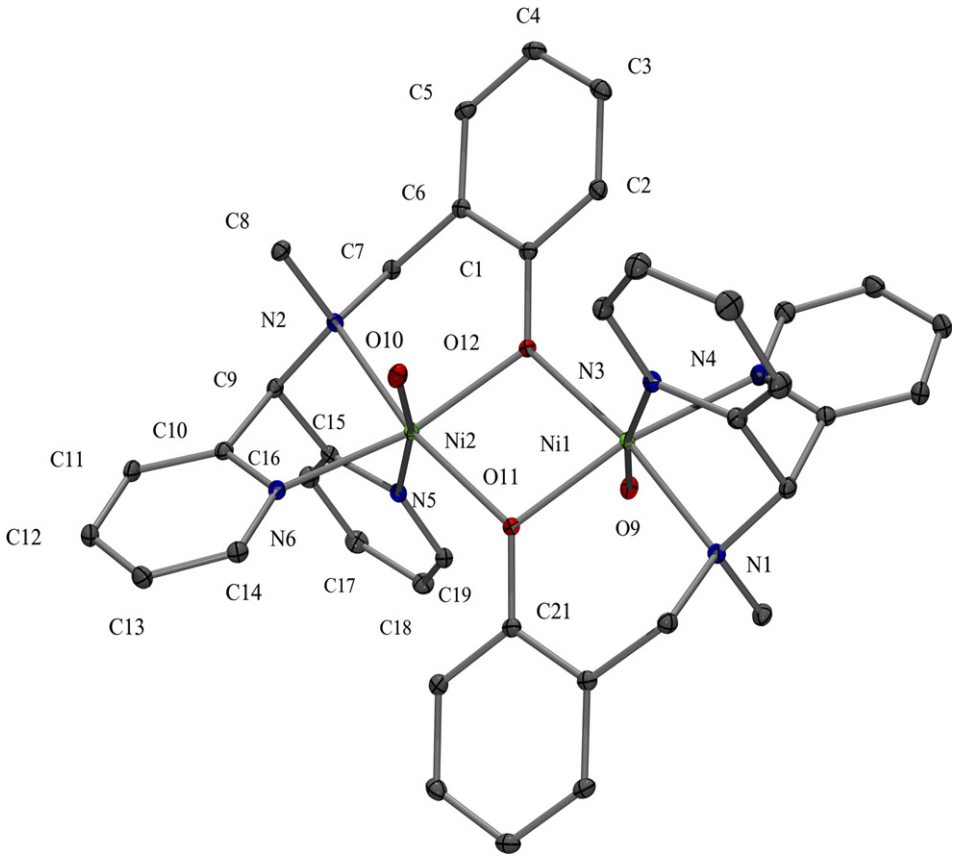


Fig. 4. The ORTEP diagram (30% ellipsoids) of $[Ni(dpmap)(H_2O)]_2(ClO_4)_2$ (cation shown without hydrogen atoms).

Table 2
Selected bond lengths (Å) and angles (°) for $[Ni(dpmap)(H_2O)]_2(ClO_4)_2 \cdot 3(CH_3)_2CO$

| | | | |
|---|---|---|---|
| Ni(1)–O(12) | 2.0156(12) | N(2)–C(8) | 1.478(2) |
| Ni(1)–O(11) | 2.0603(12) | N(2)–C(9) | 1.485(2) |
| Ni(1)–N(1) | 2.0926(15) | N(2)–C(7) | 1.492(2) |
| Ni(1)–O(9) | 2.0960(13) | N(5)–C(19) | 1.342(2) |
| Ni(1)–N(3) | 2.1018(15) | N(5)–C(15) | 1.347(2) |
| Ni(1)–N(4) | 2.1609(15) | N(6)–C(14) | 1.342(2) |
| Ni(2)–O(11) | 2.0391(12) | N(6)–C(10) | 1.349(2) |
| Ni(2)–O(12) | 2.0616(12) | Ni(2)–N(6) | 2.1208(15) |
| Ni(2)–N(2) | 2.1064(15) | Ni(2)–N(5) | 2.1238(15) |
| Ni(2)–O(10) | 2.1107(13) | N(1)–C(28) | 1.481(2) |
| O(11)–C(21) | 1.341(2) | N(1)–C(29) | 1.485(2) |
| N(4)–C(34) | 1.342(2) | N(1)–C(27) | 1.492(2) |
| N(4)–C(30) | 1.347(2) | N(3)–C(39) | 1.342(2) |
| | | N(3)–C(35) | 1.346(2) |
| O(12)–Ni(1)–O(11) | 78.59(5) | Ni(1)–O(9)–H(9A) | 116.3(17) |
| O(12)–Ni(1)–N(1) | 170.48(5) | Ni(1)–O(9)–H(9B) | 110.6(17) |
| O(11)–Ni(1)–N(1) | 92.14(5) | H(9A)–O(9)–H(9B) | 104(2) |
| O(12)–Ni(1)–O(9) | 86.26(5) | C(21)–O(11)–Ni(2) | 130.94(11) |
| O(11)–Ni(1)–O(9) | 90.29(5) | O(11)–Ni(2)–O(12) | 78.03(5) |
| N(1)–Ni(1)–O(9) | 96.04(5) | O(11)–Ni(2)–N(2) | 167.57(5) |
| O(12)–Ni(1)–N(3) | 99.19(5) | O(12)–Ni(2)–N(2) | 90.54(5) |
| O(11)–Ni(1)–N(3) | 99.65(5) | O(11)–Ni(2)–O(10) | 87.51(5) |
| N(1)–Ni(1)–N(3) | 80.08(6) | O(12)–Ni(2)–O(10) | 89.92(5) |
| O(9)–Ni(1)–N(3) | 169.42(6) | N(2)–Ni(2)–O(10) | 97.45(5) |
| O(12)–Ni(1)–N(4) | 110.30(5) | O(11)–Ni(2)–N(6) | 112.32(5) |
| O(11)–Ni(1)–N(4) | 170.35(5) | O(12)–Ni(2)–N(6) | 168.55(5) |
| N(1)–Ni(1)–N(4) | 79.10(6) | N(2)–Ni(2)–N(6) | 79.53(6) |
| O(9)–Ni(1)–N(4) | 86.66(5) | O(10)–Ni(2)–N(6) | 85.77(5) |
| N(3)–Ni(1)–N(4) | 82.95(6) | O(11)–Ni(2)–N(5) | 97.12(5) |
| C(21)–O(11)–Ni(1) | 124.45(11) | O(12)–Ni(2)–N(5) | 101.29(5) |
| Ni(2)–O(11)–Ni(1) | 101.31(5) | N(2)–Ni(2)–N(5) | 80.18(6) |
| C(34)–N(4)–C(30) | 118.02(16) | O(10)–Ni(2)–N(5) | 168.52(5) |
| C(34)–N(4)–Ni(1) | 132.46(13) | N(6)–Ni(2)–N(5) | 82.76(6) |
| C(30)–N(4)–Ni(1) | 109.31(12) | C(1)–O(12)–Ni(1) | 130.46(11) |
| C(8)–N(2)–C(9) | 109.84(13) | C(1)–O(12)–Ni(2) | 124.65(11) |
| C(8)–N(2)–C(7) | 109.03(13) | Ni(1)–O(12)–Ni(2) | 102.07(5) |
| C(9)–N(2)–C(7) | 110.02(13) | N(4)–C(34)–C(33) | 122.66(18) |
| C(8)–N(2)–Ni(2) | 118.75(11) | N(2)–C(9)–C(15) | 109.04(14) |
| C(9)–N(2)–Ni(2) | 97.84(10) | N(2)–C(9)–C(10) | 107.60(13) |
| C(7)–N(2)–Ni(2) | 110.73(10) | C(15)–N(5)–Ni(2) | 109.72(11) |
| C(19)–N(5)–Ni(2) | 132.12(12) | C(14)–N(6)–C(10) | 118.55(15) |
| C(14)–N(6)–Ni(2) | 131.35(12) | C(27)–N(1)–Ni(1) | 110.68(10) |
| C(10)–N(6)–Ni(2) | 109.86(11) | C(39)–N(3)–C(35) | 118.43(15) |
| C(28)–N(1)–Ni(1) | 117.14(11) | C(39)–N(3)–Ni(1) | 131.01(12) |
| C(29)–N(1)–Ni(1) | 98.61(10) | C(35)–N(3)–Ni(1) | 110.31(12) |

### 3.2. Electronic spectrum

The visible spectrum of the complex shows the typical three bands of octahedral nickel(II) with the $^3T_{2g} \leftarrow {}^3A_{2g}$ and $^3T_{2g}(F) \leftarrow {}^3A_{2g}$ transitions occurring at 905 nm (11 050 $cm^{-1}$), and 636 nm (15 700 $cm^{-1}$). The third band, 310 nm (32 000 $cm^{-1}$), is ~50% higher in intensity than the two lower energy transitions; this intensity is typical for bands that are a result of mixing of LMCT with the $^3T_{1g}(P) \leftarrow {}^3A_{2g}$ transition [30–32]. The intensity of the $^3T_{2g} \leftarrow {}^3A_{2g}$ transition is higher than is generally found in octahedral nickel(II). This effect has been observed in nickel(II) complexes with asymmetric ligand fields [33,34] and betokens the need for inclusion of zero-field splitting

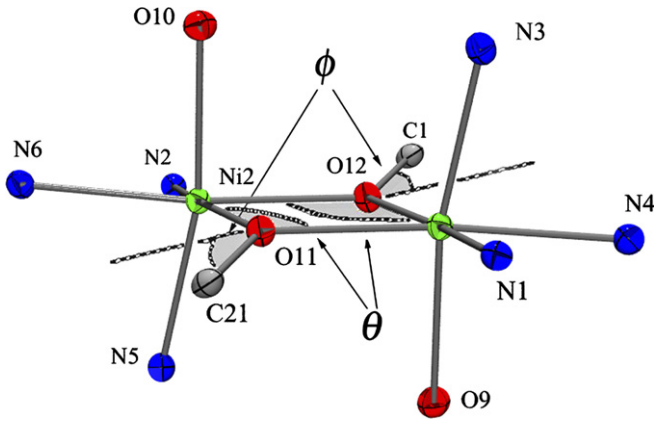


Fig. 5. ORTEP Diagram of the $Ni(N_3O_2)_2$ core in $[Ni(dpmap)(H_2O)]_2(ClO_4)_2$ ($\theta$, $\phi$, are the Ni2–O–Ni1 and the out of plane bridging, respectively).

to adequately describe the magnetic properties of this system (*vide infra*). The values of 10 *Dq* (11 050 $cm^{-1}$) and *B* (478 $cm^{-1}$) were obtained using Lever's transition energy ratio [26,35,36]. The reduction in the Racah *B* value as evidenced from small values of $\beta$ ($B_{complex}/B_{free\ ion}$) = 0.442 indicates the presence of ~56% covalency in the nickel(II)–ligand bonds. The increased covalency results in delocalization of electron density onto the ligand framework [37].

### 3.3. Magnetic properties

The variable temperature (VT) magnetic susceptibility, as $\chi_m T$ versus *T* of $[Ni(dpmap)(H_2O)]_2(ClO_4)_2 \cdot 3(CH_3)_2CO$ is shown in Fig. 6. The value of $\chi_m T$ is 2.80 $cm^3\ mol^{-1}$ K at 300 K, which is typical for two non-interacting nickel(II) ions ($g > 2.0$). The $\chi_m T$ slowly falls off upon cooling to a value of 2.36 $cm^3\ mol^{-1}$ K at 13 K, after which the values rapidly decrease to a value of 1.3 $cm^3\ mol^{-1}$ K at 2.5 K. The low temperature data indicates the presence of combination of zero-field splitting and weak intermolecular antiferromagnetic exchange between the nickel(II) centers. The variable temperature susceptibility of nickel(II) dimers can be described using an isotropic exchange Hamiltonian, $\mathscr{H} = -2J\hat{S}_1 \cdot \hat{S}_2$. Applying Kambe's method [38] to a dinuclear nickel(II) system results in the energy expression, $E(S_T) = -J[S_T(S_T+1) - S_1(S_1+1) - S_2(S_2+1)]$ where $S_T$ is the total energy of the system and $S_1$ and $S_2$ are the spins on each nickel(II) ion. $S_T$ can take on values of $S_1 + S_2$, $S_1 + S_2 - 1, \ldots, |S_1 - S_2|$. Which results in $S_T = 2, 1, 0$ states for nickel(II) ($S_1 = S_2 = 1$) with the following $E(S_T)$ states: $E(2) = 2J$, $E(1) = -2J$ and $E(0) = -4J$. Introduction of the energy terms of each $S_T$ state into the VanVleck equation results in the following equation for the molar susceptibility shown below.

$$\chi_m = \frac{Ng^2\beta^2}{3kT} \frac{24e^{-6J/kT} + 6e^{2J/kT}}{5e^{-6J/kT} + 36e^{2J/kT} + e^{-4J/kT}} \quad (1)$$

The parameters *N*, $\beta$, and *K* have their usual meanings. *J* is the exchange constant ($cm^{-1}$).

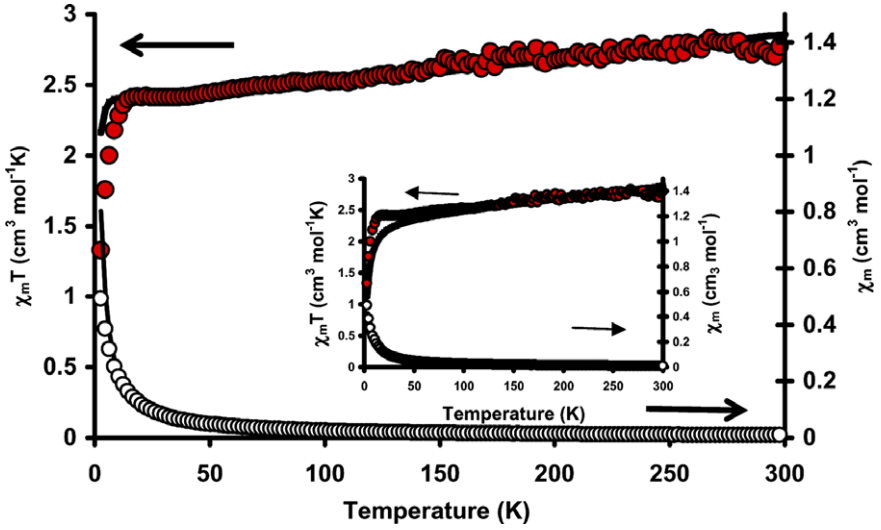


Fig. 6. The variable temperature (VT) magnetic susceptibility data for $[Ni(dpmap)(H_2O)]_2(ClO_4)_2 \cdot 3(CH_3)_2CO$.

However, in dinuclear nickel(II) systems with only weak antiferromagnetic exchange, zero-field splitting (ZFS) needs to be included in the magnetic exchange model to accurately describe the low temperature magnetic data. A method for the incorporation of zero-field splitting (ZFS) was developed for a $(Fe^{2+})_2$ [39] system and can generalized to any polynuclear system. Each $S_T$ state is split into their respective $\pm M_S$ levels.

Applying a modified Hamiltonian, $\mathscr{H} = [-2J\widehat{S}_1 \cdot \widehat{S}_2] + D\left[M_S^2 - \frac{1}{3}S(S+1)\right]$ to the above states results in a set of seven states ($M_S \pm 2$, 0 for $E(2)$, $M_S \pm 1$, 0 for $E(1)$ and $E(0)$), which depend on the magnitude and sign of $D$. The resulting susceptibility equation is:

$$\chi_m = \frac{Ng^2\beta^2}{3kT} \frac{24e^{(4J-2D)/kT} + 6e^{(4J+D)/kT} + 6e^{-\left(2J+\frac{1}{3}D\right)/kT}}{2e^{(4J-2D)/kT} + 2e^{(4J+D)/kT} + e^{(4J+2D)/kT} + 2e^{-\left(2J+\frac{1}{3}D\right)/kT} + e^{-\left(2J-\frac{2}{3}D\right)/kT} + 1} + N\alpha \quad (2)$$

Least-square fitting of all data led to $J = -0.85 \pm 0.37\ cm^{-1}$, $D = -1.6 \pm 0.8\ cm^{-1}$, $g = 2.26 \pm 0.02$ and $N\alpha = 18 \pm 2 \times 10^{-4}$. Exclusion of the $D$ term resulted in almost identical values for $J$, $g$ and $N\alpha$, however a non-zero $D$ resulted in smaller uncertainties and improvement in the overall fit. The fitting parameters are consistent with a weakly antiferromagnetically coupled dinuclear nickel(II) complex with a quasi-octahedral coordination environment (*vide supra*).

Please note that we advocate fitting VT magnetic data as $\chi_m T$, and then plotting both the $\chi_m T$ and $\chi_m$ forms to check for consistence in the fit. As can be seen from Fig. 6, the experimental $\chi_m$ fit with both $D = 0$ and a non-zero value of $D$ produce an excellent fit. However, when the data is plotted as $\chi_m T$ can the differences between the two fits become apparent. The effect of $D$ in this system cannot be overlooked, as shown in Fig. 7, zero-field splitting places the $M_S = 1$ level of the $\langle 1\,1\rangle$ state only 0.1 $cm^{-1}$ above the $\langle 0\,1\rangle$ state. This allows for rapid population of the $\langle 1\,1\rangle$ state even at 3 K. Application of Boltzmann statistics to the $M_S$ levels indicated that at 3 K the $\langle 0\,1\rangle$ ground state is 33.5% populated, the $M_S = -1$ level of the $\langle 1\,1\rangle$ state is 31.8% populated.

The variable field (VF) magnetization and AC susceptibility (field cooled, FC; and zero-field cooled, ZFC; both at 3 K) measurements also provide evidence in support of substantial population of the $\langle 1\,1\rangle$ state at low temperature. VF magnetization data suggests the presence of antiferromagnetic coupling, as the experimental points lie below the theoretical curve (Brillouin function) for $S = 1$ (Fig. 8). Field-cooled AC susceptibility measurements further indicate the presence of antiferromagnetic interactions ($\chi'$ peak at (Fig. 9) [40]. In contrast, the presence of only a $\chi''$ peak and the steady increase of the $\chi'$ component in the zero-field cooled data are indicators of ZFS effects. Therefore, the low-temperature interactions present in $[Ni(dpmap)(H_2O)]_2(ClO_4)_2 \cdot 3(CH_3)_2CO$ are a combination of zero-field splitting and antiferromagnetic exchange phenomenon.

Most of the magnetostructural correlations for dinuclear nickel(II) complexes are based on the work of Nanda and coworkers [41]. This work, based on a series of centrosymmetric octahedral and square pyramidal dinickel(II) complexes, indicates a linear relationship between $J$ and the Ni–O–Ni bridging angles. Furthermore a bridging angle of 97° is the crossover point between ferromagnetic and antiferromagnetic coupling. In nickel tetramers, magnetostructural correlations are quite strong [42] and these correlations predict that when the Ni–Ni interactions are

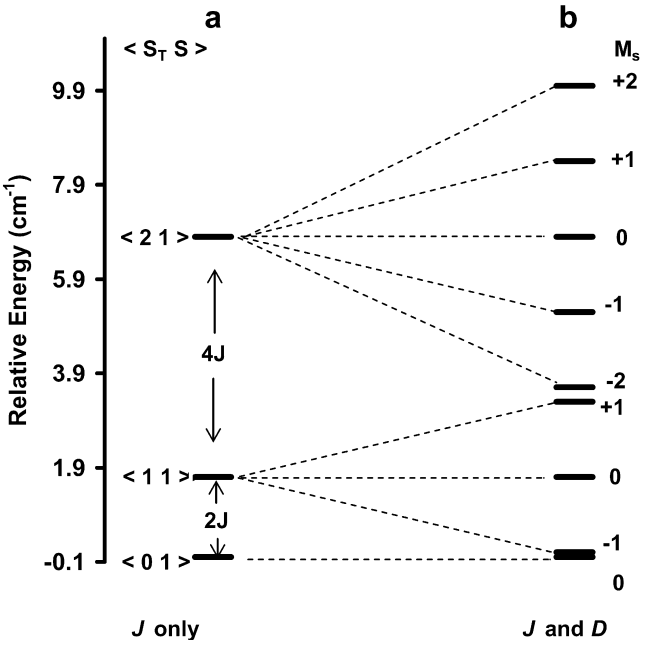


Fig. 7. Energy levels: (a) coupling only, (b) coupling and ZFS.

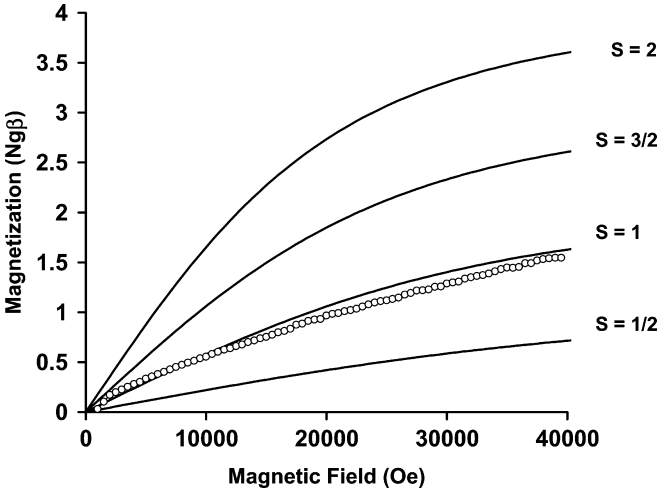


Fig. 8. Variable field of $[Ni(dpmap)(H_2O)]_2(ClO_4)_2$ (at 3 K). The solid lines are plot of the Brillouin function ($g = 2.0$) for various $S$ values.

orthogonal, ferromagnetic interactions dominate (interactions between orthogonal orbitals (Ni(1) $d_{x^2-y^2}$ and Ni(1) $d_{z^2}$, or vice versa). Likewise, when the nickel-nickel interactions approach parallel, strong antiferromagnetic interactions occur (Ni(1) $d_{x^2-y^2}$ and Ni(1) $d_{x^2-y^2}$) or (Ni(1) $d_{z^2}$ and Ni(2) $d_{z^2}$). Since the Ni–O–Ni angle in $[Ni(dpmap)(H_2O)]_2(ClO_4)_2$ is on average 101.70 Å, the complex should accordingly display moderately strong antiferromagnetic exchange ($J \sim -35\ cm^{-1}$) instead of the extremely weak antiferromagnetism which is actual observed. The majority of the reported phenoxo-bridged dinickel complexes enforce a planarity geometry about the bridging oxygen donor and thus result in strong antiferromagnetic interactions ($-20 > J > -100\ cm^{-1}$) between the nickel centers. Clear-cut correlations present in dinickel(II) systems with enforced planar bridges fail once this restriction is removed [43]. Cano and coworkers have suggested that the out of plane angle ($\phi$) (*vide supra*) is of as much importance as M–X–M angle ($\theta$) in determining the sign and direction of the $J$ value [44]. In $[Ni(dpmap)(H_2O)]_2(ClO_4)_2$, the phenolato-rings are above and below the $NiO_2Ni$ plane by ~15° and thus prevent an adequate pathway for superexchange, and resulting in the observed weak antiferromagnetism.

Previous studies of urease model complexes also suggest that only very weak antiferromagnetic exchange interactions ($0 > J > -5\ cm^{-1}$) probably exist in urease due to the type and angles of bridging donors present. Such small coupling constants would be extremely difficult to measure in protein samples and may have been interpreted as a non-interaction in the native enzyme [45].

### 3.4. DFT calculations

DFT calculations on the complex cation, $[Ni(dpmap)(H_2O)]_2^{2+}$ (from X-ray crystallographic coordinates) were performed to gather insight into the electronic structure

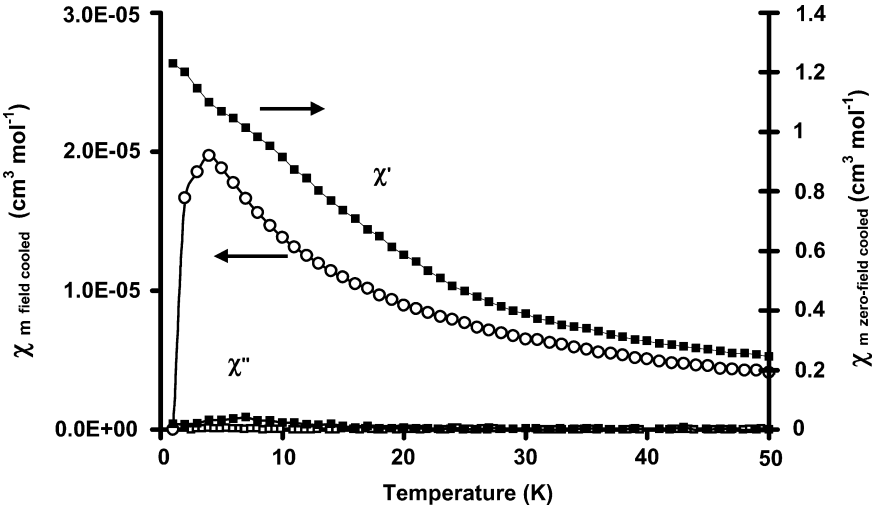


Fig. 9. The in phase ($\chi'$) and out of phase ($\chi''$) field cooled (FC) and zero field cooled (ZFC) AC susceptibility measurements in $Ni(dpmap)(H_2O)]_2(ClO_4)_2$.

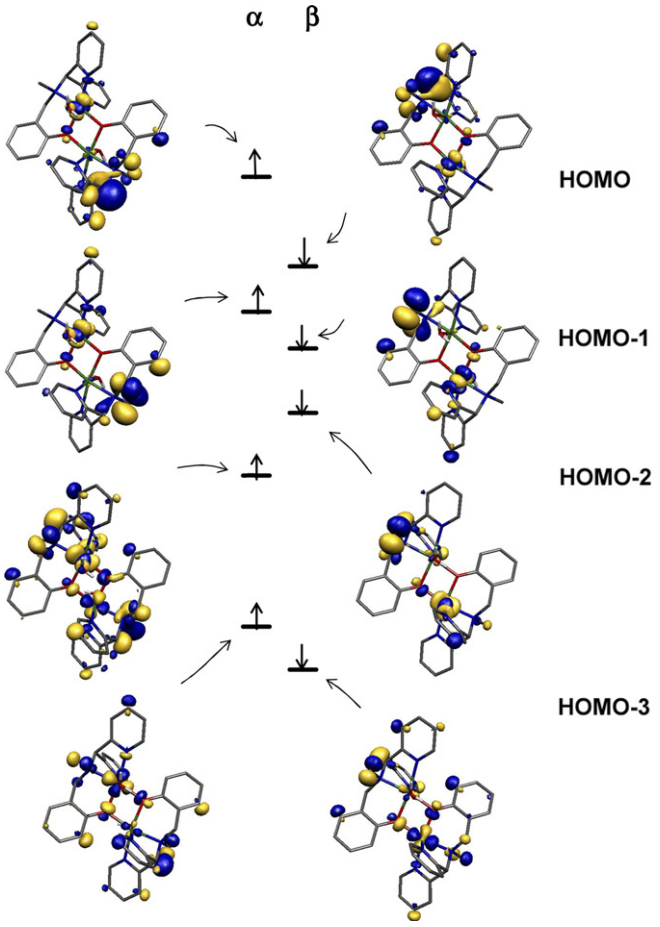


Fig. 10. Qualitative broken symmetry frontier orbital diagram (from DFT) for $[Ni(dpmap)(H_2O)]_2^{2+}$ $S$(overlap integral) = 0.027 at the HOMO and 0.071 at HOMO − 1 levels.

and the source of the weak antiferromagnetism present in the dimer.

Both high-spin (HS) and broken-symmetry (BS) spin-unrestricted were performed. The HS ($S = 6$) state was found to be lower in energy by 0.0112 eV relative to the BS ($S = 0$) state. This result betokens weak ferromagnetic interactions between the nickel centers as evidenced by a calculated magnetic coupling constant ($J$) (*vide supra*) of $+24.30\ cm^{-1}$. However, the experimentally determined coupling constant ($-0.85\ cm^{-1}$) is different in magnitude and sign. Little credence can be placed on the DFT calculated value, as most theoretical estimates of $J$ for weakly coupled systems often yield values significantly different in both sign and magnitude. It is well know that magnetic coupling constants ($J$ values) are often overestimated in broken-symmetry DFT calculations [46–49]. Magnetic exchange pathways are best described as resulting from configuration interactions between individual wavefunctions, which are not strictly part of DFT [50,51]. However, the magnetic orbitals as derived from a broken-symmetry solution are useful in understanding mechanisms of spin exchange in polynuclear complexes [52], since the molecule is treated as two weakly antiferromagnetically coupled monomeric complexes [53]. In the broken symmetry state, the $\alpha$ and $\beta$ electrons are localized on different atoms, thus resulting in substantial interactions between the spins on each metal center by the p-orbitals of the bridging atoms.

The corresponding orbital transformation [54,55] provides insight into the nature of the solution. The HOMO and HOMO − 1 levels have overlap integrals of 0.027 and 0.071, respectively. Small values of the overlap integral ($S \ll 1$) for corresponding orbitals indicate a large degree of spin polarization and thus signal the nonorthogonal magnetic orbital pairs. The spatial overlap of the SOMOs is consistent with weak antiferromagnetic coupling. Analysis of the Mulliken spin populations (Table 4) indicates the presence of weak antiferromagnetic coupling between Ni(1) and Ni(2), where the spin densities are −1.332 and +1.338, respectively, the spin density data suggested that little of the spin density is delocalized onto the adjacent donor atoms. Furthermore the formal oxidation state of each nickel ion (Ni(2) and (Ni(2) = +2.31) are consistent with the Mulliken spin populations.

In $O_h$ symmetry, nickel(II) has a ground state configuration of $(t_{2g})^6(e_g)^2$. When two nickel(II) centers are linked in a dimer, four molecular orbitals having mainly $e_g$ ($d_{z^2}$ and $d_{x^2-y^2}$) character result. The orthogonal, localized orbitals on each nickel center are formed from these four MOs [56]. To attain effective antiferromagnetically coupling the

Table 3
Energies and molecular orbital compositions (%) for relevant nickel and bridging phenolate oxygen donors

| MO | Energy (eV) | Ni(1) | Ni(2) | O(11) | O(12) | Ligand[a] |
|---|---|---|---|---|---|---|
| 179 α (HOMO) | −0.4147 | 0.5 ($d_{xz}$), 0.8 ($d_{yz}$), 1.2 ($d_{xy}$) | 1.0 ($d_{xz}$), 0.6 ($d_{yz}$) | 9.0($p_y$), 1.3 ($p_z$) | 0.6 ($p_y$) | 78.4 |
| 179 β (HOMO) | −0.4170 | 0.7 ($d_{xy}$) | 0.6 ($d_{xz}$), 2.6 ($d_{xy}$), 1.0 ($d_{x^2-y^2}$) | 7.5($p_y$), 1.3 ($p_z$) | 2.0 ($p_y$) | 77.3 |
| 178 α | −0.4191 | 0.5 ($d_{yz}$), 1.3 ($d_{xy}$), 1.1 ($d_{x^2-y^2}$) | 0.9 ($d_{xy}$) | | 6.8 ($p_y$), 1.5 ($p_z$) | 81.6 |
| 178 β | −0.4176 | | 2.1 ($d_{yz}$), 0.5 ($d_{xy}$) | | 7.1 ($p_y$) | 80.2 |
| 177 α | −0.4245 | 0.5 ($d_{z^2}$),1.2 ($d_{x^2-y^2}$) 2.0 ($d_{xy}$) | 0.7 ($d_{xz}$) | 0.8 ($p_x$) | 1.5 ($p_x$), 8.3 ($p_y$), 1.9 ($p_z$) | 77.1 |
| 177 β | −0.4224 | | 0.9 ($d_{z^2}$), 1.2 ($d_{x^2-y^2}$), 0.6 ($d_{xz}$), 1.4 ($d_{xy}$) | 1.6 ($p_x$), 1.7 ($p_z$), 7.3 ($p_y$) | 1.1 ($p_y$) | 87.4 |
| 176 α | −0.4294 | 0.5 ($d_{z^2}$) | 1.6 ($d_{xz}$), 1.8 ($d_{xy}$) | 1.1 ($p_x$), 1.6 ($p_y$) | | 87.8 |
| 176 β | −0.4308 | 1.4 ($d_{xz}$), 2.0 ($d_{xy}$) | 0.7 ($d_{z^2}$), | 1.6($p_x$), 1.5 ($p_y$) | 1.3 ($p_x$), 1.5 ($p_y$) | 83.0 |

[a] Rest of the ligand taken together.

Table 4
Mulliken spin densities of the nickel centers and coordinated atoms

| Atom | Spin population |
|---|---|
| Ni(1) | −1.33 |
| Ni(2) | 1.34 |
| N(2) | −0.06 |
| N(3) | −0.05 |
| N(4) | −0.05 |
| N(6) | 0.05 |
| N(5) | 0.05 |
| N(1) | 0.06 |
| O(10) | −0.04 |
| O(12) | −0.01 |
| O(11) | 0.01 |
| O(9) | 0.04 |

two nickel(II) centers, exchange pathways in both the $x$–$y$ plane and $x$-directions need to be provided. As can be seen from Fig. 10 and Table 3, the superexchange pathways between the nickel centers are primarily limited to orbitals 177 $\alpha$ and $\beta$, whereas the remaining orbitals show a larger degree of spin localization, which is consistent for systems, such as $[Ni(dpmap)(H_2O)]_2(ClO_4)_2 \cdot 3(CH_3)_2CO$ with very weak AF coupling (see Table 4).

## Acknowledgements

M.J.P. and D.M.T. acknowledge La Salle University for support. This work was supported by a Summer Faculty Research Grant (2005) from the School Arts and Sciences, La Salle University. The Smart Apex diffractometer was funded by NSF Grant 0087210, by Ohio Board of Regents Grant CAP-491, and by YSU.

## Appendix A. Supplementary material

CCDC 623322 contains the supplementary crystallographic data for this paper. These data can be obtained free of charge via http://www.ccdc.cam.ac.uk/conts/retrieving.html, or from the Cambridge Crystallographic Data Centre, 12 Union Road, Cambridge CB2 1EZ, UK; fax: (+44) 1223-336-033; or e-mail: deposit@ccdc.cam.ac.uk. Supplementary data associated with this article can be found, in the online version, at doi:10.1016/j.ica.2006.11.008.

## References

[1] F. Meyer, E. Kaifer, P. Kircher, K. Heinze, H. Pritzlow, Chem. Eur. J. 5 (1999) 1617.
[2] D. Volkmer, B. Hommerich, K. Griesar, W. Haase, B. Krebs, Inorg. Chem. 35 (1996) 3792.
[3] A.M. Barrios, S.J. Lippard, Inorg. Chem. 40 (2001) 1250.
[4] U. Erlmer, W. Grabarse, S. Shima, M. Goubeaud, Curr. Opin. Struct. Biol. 8 (1998) 749.
[5] E. Jabri, M.B. Carr, R.P. Hausinger, P.A. Karplus, Science 268 (1995) 998.
[6] P.A. Clark, D.E. Wilcox, Inorg. Chem. 28 (1989) 1326.
[7] E.P. Day, J. Peterson, M.S. Sendova, M.J. Todd, R.P. Hausinger, Inorg. Chem. 32 (1993) 634.
[8] Y. Hosokawa, H. Yamane, Y. Nakao, K. Matsumoto, S. Takamizawa, W. Mori, S. Suzuki, H. Kimoto, Inorg. Chim. Acta. 283 (1998) 118.
[9] H. Hu, Y. Liu, D. Zhang, C. Liu, J. Mol. Struct: Theochem. 546 (2001) 73.
[10] R.M. La Crois, Ph.D. Thesis, University of Groningen, 2000.
[11] J. Brinksman, R. La Crois, B.L. Feringa, M.I. Donnoli, C. Rosini, Tetrahedron Lett. 42 (2001) 4049.
[12] J. Vicario, R. Eelkema, W.R. Browne, A. Meetsman, R.M. La Crois, B.L. Feringa, Chem. Commun. 31 (2005) 3936.
[13] A.L. Spek, Acta Cryst. A46 (1990) C34.
[14] A.L. Spek, PLATON: A Multipurpose Crystallographic Tool, Ulricht University, Ulricht, The Netherlands, 2005.
[15] ARGUSLAB 4.0.1, Mark A. Thompson, Planaria Software LLC, Seattle, W. <http://www.arguslab.com>.
[16] Bruker, SAINT (Version 6.02), SMART for WNT/2000 (Version 5.625), Bruker AXS Inc., Madison, Wisconsin, USA, 1997.
[17] G.M. Sheldrick, SHELXS97 and SHELXL97, University of Göttingen, Germany, 1997.
[18] F. Neese, ORCA – An *ab initio*, Density Functional and Semiempirical Program Package, Version 2.4, Revision 45, Max Planck Institut für Bioanorganische Chemie, Mülheim, 2003.
[19] J.P. Perdew, J.A. Chevary, S.H. Vosko, K.A. Jackson, M.R. Pederson, D.J. Singh, C. Fiolhais, Phys. Rev. B. 46 (1992) 6671.
[20] A. Schaefer, H. Horn, R. Ahlrichs, J. Chem. Phys. 97 (1992) 2571.
[21] R. Ahlrichs and coworkers, unpublished results.
[22] K. Eichkorn, O. Treutler, H. Ohm, M. Haser, R. Ahlrichs, Chem. Phys. Lett. 240 (1995) 283.
[23] K. Eichkorn, F. Weigend, O. Treutler, R. Ahlrichs, Theor. Chem. Acc. 97 (1997) 119.
[24] C.J. Van Alsenoy, J. Comp. Chem. 9 (1988) 620.
[25] R.A. Kendall, H.A. Früchtl, Theor. Chem. Acc. 97 (1997) 158.
[26] O. Treutler, R. Ahlrichs, Theor. Chem. Acc. 97 (1997) 119.
[27] K. Yamaguchi, Y. Takahara, T. Fueno, in: V.H. Smith (Ed.), Applied Quantum Chemistry, Reidel, Dordrecht, 1986.
[28] P. Flükiger, H.P. Lüthi, S. Portmann, J. Weber, MOLEKEL 4.3, Swiss Center for Scientific Computing, Manno, Switzerland, 2000.
[29] Stefan Portmann, Hans Peter Lüthi, CHIMIA 54 (2000) 766.
[30] S.K. Dutta, K.K. Nanda, U. Florke, M. Bhadbhade, K. Nag, J. Chem. Soc., Dalton Trans. (1996) 2371.
[31] M.J. Prushan, A.W. Addison, R.J. Butcher, Inorg. Chim. Acta 300–302 (2000) 992.
[32] S.R. Cooper, S.C. Rawle, J.R. Hartman, E.J. Hintsa, G.A. Admans, Inorg. Chem. 27 (1988) 1209.
[33] R. Das, K.K. Nanda, K. Venkatsubramanian, P. Paul, K. Nag, J. Chem. Soc., Dalton Trans. (1992) 1253.
[34] A. McAuley, D.G. Fortier, D.H. Macartney, T.W. Whitcombe, C. Xu, J. Chem. Soc., Dalton Trans. (1994) 2071.
[35] J.G. Gilbert, A.W. Addison, R.J. Butcher, Inorg. Chim. Acta 308 (2000) 22.
[36] A.B.P. Lever, Inorganic Electronic Spectroscopy, 2nd edn., Elsevier, Amsterdam, 1984.
[37] S. Singh, V. Mishra, J. Mukherjee, N. Seethalekshmi, R. Mukherjee, Dalton Trans. (2003) 3392.
[38] K. Kambe, J. Phys. Soc. Jpn. 5 (1950) 48.
[39] V.V. Pavlishchuk, M.J. Prushan, A.W. Addison, Theor. Exper. Chem. 41 (2005) 229.
[40] S. Blundell, Magnetism in Condensed Matter, Oxford University Press, USA, 2001. Antiferromagnetism is characterized by the presence of a peak in the in-phase ($\chi'$) and a zero out of phase ($\chi''$) component. Whereas, a ferromagnetic transition results in a peak in $\chi'$ vs. temperature plot and a non-zero $\chi''$ vs. temperature value. In antiferromagnets the lack of the out of phase component, which in ferromagnets results from the energy absorbed as the magnetic moment adjusts to the oscillating magnetic field.
[41] K.K. Nanda, L.K. Thompson, J.N. Bridson, K. Nag, J. Chem. Soc., Chem. Commun. (1994) 1337.

[42] V.V. Pavlishchuk, S.V. Kolotilov, A.W. Addison, M.J. Prushan, D. Schollmeyer, L.K. Thompson, T. Weyhermüller, E.A. Gorerhnik, Dalton Trans. 8 (2003) 1587.
[43] S.K. Dey, M.S. El. Fallah, J. Ribas, T. Matsushita, V. Gramlich, Inorg. Chim. Acta 357 (2004) 1517.
[44] J. Cano, G. De Munno, J.L. Sanz, R. Ruiz, J. Faus, F. Lloret, M. Julve, A. Caneschi, J. Chem. Soc., Dalton Trans. (1997) 1915.
[45] M.A. Halcrow, G. Christou, Chem. Rev. 94 (1994) 2421.
[46] C. Adamo, V. Barone, A. Benicni, F. Totti, I. Ciofini, Inorg. Chem. 38 (1999) 1996.
[47] T. Soda, Y. Kitagawa, T. Onishi, Y. Takano, Y. Shigeta, H. Nagao, Y. Yoshioka, K. Yamaguchi, Chem. Phys. Lett. 319 (2000) 223.
[48] A. Bencini, F. Totti, C.A. Daul, K. Doclo, P. Fantucci, V. Barone, Inorg. Chem. 36 (1997) 5022.
[49] X.G. Zhao, W.H. Richardson, J.-L. Chen, L. Noodleman, H.-L. Tsai, D.N. Hendrickson, Inorg. Chem. 36 (1997) 1198.
[50] O. Kahn, Molecular Magnetism, VCH publishers, New York, 1993.
[51] J. Miralles, J.P. Daudey, R. Caballol, Chem. Phys. Lett. 198 (1992) 555.
[52] J.E. Mc Grady, R. Stranger, J. Am. Chem Soc. 119 (1997) 8512.
[53] L. Noodleman, J.G. Morman Jr., J. Chem. Phys. 70 (1979) 4903.
[54] D. Herebian, K.E. Wieghardt, F. Neese, J. Am. Chem. Soc. 125 (2003) 10997.
[55] F. Nesse, J. Phys. Chem. Solids 65 (2004) 781.
[56] P.J. Hay, J.C. Thibeault, R. Hoffmann, J. Am. Chem. Soc. 97 (1975) 4884.